NANO LETTERS

Letter

pubs.acs.org/NanoLett

Illumination Angle Insensitive Single Indium Phosphide Tapered Nanopillar Solar Cell

Wai Son Ko,[†] Thai-Truong D. Tran,[†] Indrasen Bhattacharya,[†] Kar Wei Ng,[†] Hao Sun,[†,‡] and Connie Chang-Hasnain*,[†]

[†]Department of Electrical Engineering and Computer Sciences, University of California at Berkeley, Berkeley, California 94720, United States

[‡]Department of Electronic Engineering, Tsinghua University, Beijing, 100084, People's Republic of China

Supporting Information

ABSTRACT: Low cost, high efficiency photovoltaic can help accelerate the adoption of solar energy. Using tapered indium phosphide nanopillars grown on a silicon substrate, we demonstrate a single nanopillar photovoltaic exhibiting illumination angle insensitive response. The photovoltaic employs a novel regrown core−shell p-i-n junction to improve device performance by eliminating shunt current paths, resulting in a high V_{OC} of 0.534 V and a power conversion efficiency of 19.6%. Enhanced broadband light absorption is also demonstrated over a wide spectral range of 400−800 nm.

KEYWORDS: *nanopillar, nanowire, solar cell, angle insensitive, radial junction, silicon substrate*

Downloaded by UNIV OF CALIFORNIA BERKELEY at 15:50:55:676 on June 11, 2019
from https://pubs.acs.org/doi/10.1021/acs.nanolett.5b00756.

The III−V compound semiconductor nanowires have been under investigation due to their reduced material consumption while maintaining excellent light absorption.[1] Lowering cost while sustaining the III−V efficiency advantage necessitates the growth of defect-free nanowire solar cells directly on cheaper foreign substrates,[2−5] such as crystalline silicon or polysilicon, both workhorses in large scale photovoltaics. Unfortunately, lattice mismatch constrains the dimensions of coherent axial nanowire growth of III−V materials on dissimilar substrates, using conventional methods such as the vapor−liquid−solid technique and other catalyst assisted techniques.[1,6] Demonstrations of efficient device operation and light absorption beyond ray optics limitations, while important, have been limited to expensive native substrates, where axial growth has been radially scaled, often requiring additional surface treatment to reduce dark current.[7−11] Promising work with lattice mismatched substrates has been achieved by first growing a very thin (∼100−200 nm) axial nanowire template and overgrowing in the radial growth mode at very different growth temperatures or different precursor flow rates.[4,5,12,13] The literature indicates that it is quite challenging to obtain a good interface and lattice match with radial overgrowth.[4,12] The growth rate of the shell layer and the dependence of crystal phase on growth conditions can also be major constraints.[13]

We have introduced a novel purely core−shell growth technique to grow monolithic micro/nanopillars in the Wurtzite phase with morphologies as diverse as GaAs on Sapphire (46% lattice mismatch),[14] (Al,In)GaAs on Si (4−6% lattice mismatch),[15] and InP on poly- and monocrystalline Si (8% lattice mismatch).[16,17] Horizontal termination of defects at the pillar base leads to a pristine Wurtzite phase in the nanopillar body.[18] In situ dopant incorporation can be used to define a core−shell p-i-n junction and heterostructures, which is advantageous both in terms of carrier collection as well as surface passivation. Additionally, with increasing growth time the structures can be scaled to even 1 μm in diameter and 4 μm in height, representing a two-orders of magnitude reduced surface−volume ratio compared to conventionally sized nanowires with a diameter around 100 nm. This results in a greatly reduced surface recombination current for the core−shell structure.

In this paper, we demonstrate a single-crystalline indium phosphide (InP) nanopillar solar cell directly grown and fabricated on a silicon substrate with a an open circuit voltage (V_{OC}) of 0.534 V under Air Mass 1.5 Global (AM 1.5 G) illumination at room temperature. To the best of our knowledge, this is the highest V_{OC} ever achieved for InP or GaAs nanowire/pillar solar cell grown on any foreign substrate. This high V_{OC} can be attributed to the high-quality single-crystalline InP nanopillars grown using a novel regrowth technique to drastically reduce the dark current to sub-fA/μm^2

Received: February 24, 2015
Revised: June 5, 2015
Published: June 17, 2015

 © 2015 American Chemical Society

DOI: 10.1021/acs.nanolett.5b00756
Nano Lett. 2015, 15, 4961−4967

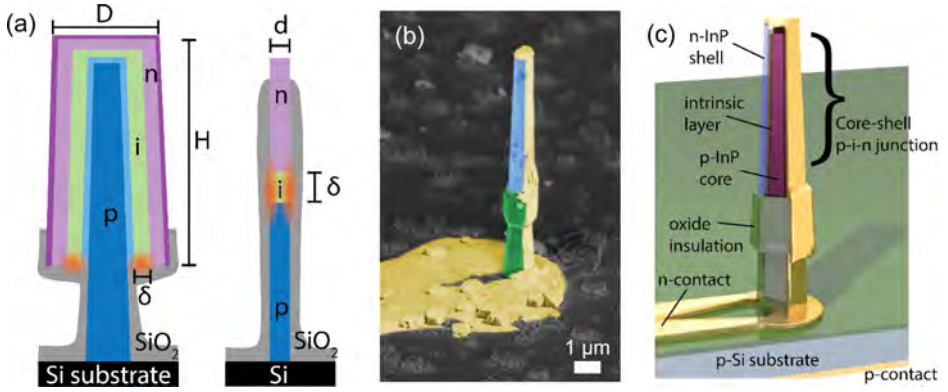

Figure 1. Single InP nanopillar solar cell. (a) Schematics of the junctions in core−shell nanopillars (left) and axial nanowires (right) with the exposed surfaces highlighted. The exposure of the depletion region to surface dangling bonds is especially harmful in terms of dark recombination current, and it can be seen that the situation is much more severe for thinner axial structures grown on non-native substrates than it is for the scalable core−shell structure from a simple analysis of what fraction of the junction surface is exposed. Schematic (b) and scanning electron micrograph (c) of single InP nanopillar solar cell fabricated on silicon substrate.

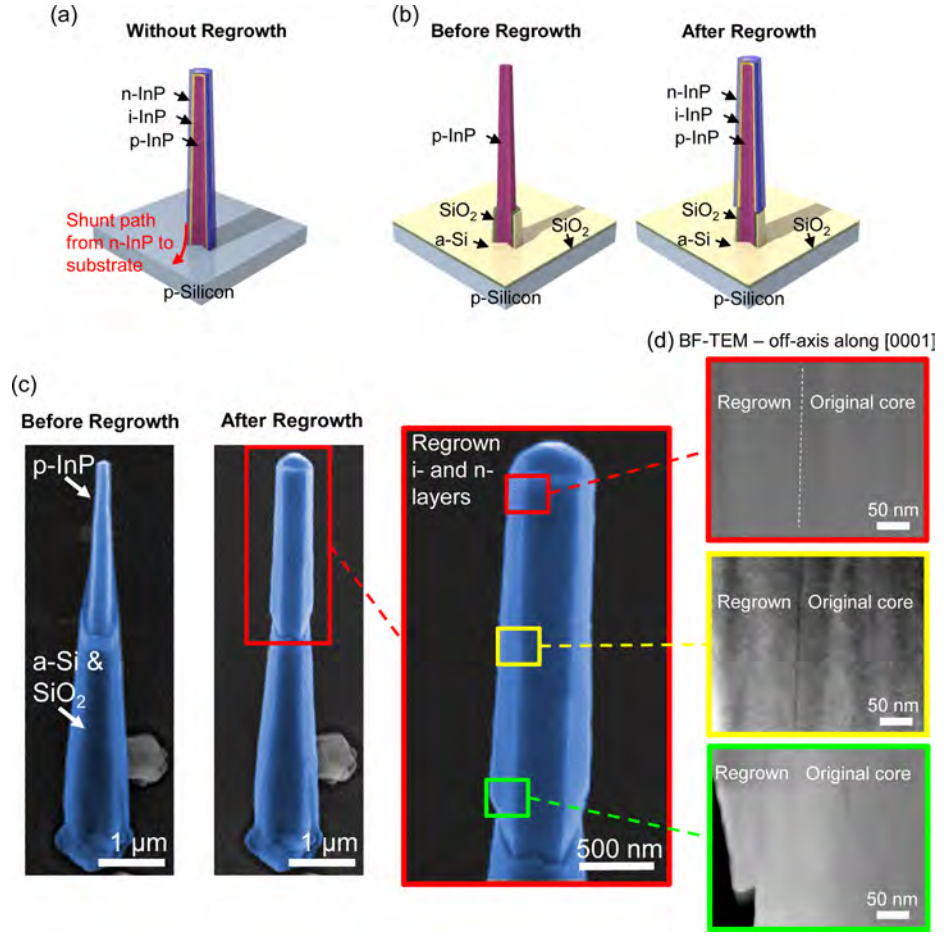

Figure 2. Regrowth on nanopillar. (a) Schematic of a nanopillar with p-i-n junction grown in one continuous growth. Since the n-InP is touching the p-silicon substrate, current can leak from the n-InP to the substrate, causing high dark current for the device. (b) Schematics of a nanopillar before and after regrowth. (c) Scanning electron micrographs of a nanopillar before and after the regrowth of i- and n-InP on p-InP. The regrown layers only grow on the top portion of the nanopillar because the bottom half of the nanopillar is masked with an amorphous silicon (a-Si) and SiO_2 mask. The zoomed in image on the right shows the smooth sidewalls of the regrown layers, suggesting that the regrown layers have excellent material quality. (d) Bright-field tunneling electron micrographs of a nanopillar taken at different locations along the nanopillar showing the junction between the regrown layers and the original nanopillar core. The image was taken at slightly off axis along the [0001] direction to show stacking dislocation more clearly. As shown in the images, the regrown layers are of excellent quality and are virtually stacking dislocation free.

levels, which is 6 orders of magnitude lower than the level of solar illumination. The tapered nanopillar sidewalls and an interesting dielectric antenna enhancement additionally allow the absorption to surpass ray optics limitations.[5,7,19,20] Another consequence is that the output current of the solar cell shows a very weak dependence on incident light angle. This makes the

DOI: 10.1021/acs.nanolett.5b00756
Nano Lett. 2015, 15, 4961−4967

solar cell insensitive to the position of the sun throughout the day and seasonal changes, reducing the need of a tracking system and the cost associated with solar output fluctuation, which lowers the levelized cost of energy by ~20%.[21] Furthermore, we present a unique tapered micropillar whose enhanced absorption with a dielectric antenna enhancement effect leads to insensitivity to angle of illumination. Together with cheaper growth substrate, less material usage, illumination angle insensitive response and the potential for high conversion efficiency, InP nanopillar solar cells are a promising path for reaching grid parity. Efficient photovoltaics built on a silicon substrate can also be used as on-chip power plants, enabling many exciting emerging applications such as environmental and biomedical sensors, retinal prosthesis[22] and optical power transfer.[23]

Material Growth and Fabrication. The efficiency of a solar cell depends strongly on its open circuit voltage, V_{OC}, which in turn depends on the ratio of short circuit current I_{SC} to dark current I_D. The former depends on the product of optical absorption (converting photons to electron−hole pairs) and the collection of electrons and holes at the contacts as current. On the other hand, the dark current is proportional to defect density and surface recombination rate. Here, excellent material quality using a regrown core−shell p-i-n junction leads to a drastically increased I_{SC}/I_D and V_{OC}.

The fabrication of the solar cell begins with the catalyst-free synthesis of wurtzite phase InP nanopillars via metal−organic chemical vapor deposition (MOCVD) on (111) silicon substrate at a low growth temperature of 450 °C.[14−18] The nanopillars grow in a unique core−shell growth mode, allowing us to demonstrate the growth of single crystalline phase, high quality material with size scalable to microns without being subjected to the nanowire critical diameter limit.[6] As the growth is in core−shell mode, radial p-i-n junction is easily formed by flowing dopants during the growth sequence. Compared to an axial junction, a core−shell p-i-n junction has two advantages: (1) a much reduced air-exposed surface area of the junction, which minimizes dark current due to defects or surface states, and (2) carrier extraction is more efficient with a reduced length at which carriers have to travel to get to the contacts.[24] The surface recombination rate for different p-i-n junction geometries on the same material system can be compared via the ratios of exposed surface to absorption volume for these structures. Surface exposure of the depletion region in a p-i-n junction is particularly unfavorable in terms of nonradiative recombination and leads to a dark recombination current of with an ideality factor of 2.[26] The most detrimental surfaces have been highlighted in red in Figure 1a. We see that the surface to volume ratio for a core−shell structure with small taper angle, can be estimated as

$$\frac{S}{V} \sim \frac{\pi D\delta}{\pi D\delta H} = \frac{1}{H} \sim \frac{1}{4\,\mu\mathrm{m}} \tag{1}$$

whereas for an axial junction a much larger fraction of the active volume is surface exposed

$$\frac{S}{V} = \frac{\pi d\delta}{\frac{1}{4}\pi d^2\delta} = \frac{4}{d} \sim \frac{4}{100\,\mathrm{nm}} \tag{2}$$

This estimation shows that the surface to volume ratio is on the order of 10^2 times higher for an axial geometry, leading to a high surface recombination current for thinner nanowires grown on lattice mismatched substrates. Including diffusion lengths in the calculation does not alter this conclusion. The absorption volume in a core−shell structure can be large without compromising on surface exposure. This geometry is then a natural choice to approach bulklike performance parameters with nano/microscale structures.

A p-i-n junction formed by the core−shell nanopillar growth method using one continuous growth, however, still suffers from significant dark current due to a shunt path to the substrate, which is illustrated in Figure 2a. To circumvent this problem, we performed a secondary growth (i.e., regrowth) to place the p-i-n junction on the top portion of a p-doped nanopillar and, hence, eliminating the shunt path. This regrowth process is schematically shown in Figure 2b. Regrowth was done by masking the bottom portion of an already grown p-type nanopillar with thin layers of silicon dioxide (SiO_2) and amorphous silicon prior to regrowth. Amorphous silicon was found to be critical to the regrowth process as it shortens the diffusion lengths of the growth precursor adatoms on the growth mask to aid thin film like deposition on the nanopillar sidewalls. More details on the preparation steps can be found in the nanopillar growth section in the Supporting Information. With regrowth, the size and location of the p-i-n junction can be controlled precisely along the length of the nanopillar. This added control and the elimination of shunt current path allow us to dramatically improve the device dark current characteristic by 6 orders of magnitude (Supporting Information Figure 3). Figure 2c shows the before and after regrowth scanning electron micrographs, showing the smooth sidewalls of a regrown nanopillar as a sign of excellent regrowth material quality. Indeed, when examined under a high-resolution transmission electron microscope (HR-TEM) (Figure 2d), the regrown junction exhibits high crystal quality over large examined sections along the length of the nanopillar, suggesting that the regrown material is virtually free of stacking dislocations. Our previous material studies also showed bright photoluminescence, greater than 1 eV Fermi level split at one sun condition,[25] and fast radiative recombination lifetime of ~300 ps at 4 K from these nanopillars.[27] When the regrowth process is completed, a typical nanopillar has a natural vertically tapered shape with an upper and lower diameter of 650 and 900 nm, respectively, and a junction length of 5.5 μm. This natural nanopillar shape produces a unique dielectric antenna effect that is further enhanced by the tapered sidewalls, facilitating enhanced absorption over a broad spectrum, which is discussed in the next section.

After regrowth, the outer n-doped layer of a single nanopillar was electrically contacted via electron beam lithography and angled Ti/Au (7 nm/150 nm) metal evaporation. The p-core contact was formed on the backside of the p-doped silicon substrate. The schematic and SEM image of such a fabricated device are shown in Figure 1. In this case, because we use thick, nontransparent metal as the n-contact on the nanopillar, less than half of the nanopillar is exposed for surface normal light capturing. Efficiency calculation is therefore normalized to the actual exposed junction area of the nanopillar, following the same method used in ref 5. More details on how the exposed area is defined can be found in Methods in the Supporting Information. In the future, the exposed area can be increased with the use of transparent electrodes, such as indium tin oxide (ITO), which has been successfully demonstrated to form good electrical contacts to InP nanowires.[7−9]

DOI: 10.1021/acs.nanolett.5b00756
Nano Lett. 2015, 15, 4961−4967

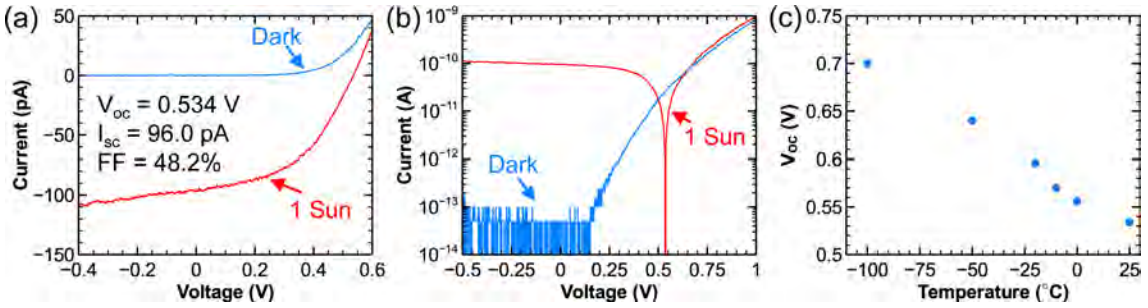

Figure 3. Single nanopillar solar cell electrical characteristics. (a,b) Room-temperature dark and 1 sun (AM 1.5 G) IV characteristics of a single InP nanopillar solar cell in linear (a) and log (b) scale. (c) V_{OC} as a function of temperature showing that the V_{OC} can reach 0.7 V at −100 °C. The temperature coefficient of V_{OC} at 1.35 mV/K is lower than that of CIGS and c-Si solar cells.[38]

Photovoltaic Measurements. The InP micropillar solar cell is tested with a solar simulator with a calibrated AM 1.5 G solar irradiation spectrum. A typical room-temperature current−voltage (I−V) characteristic under dark testing condition is shown in Figure 3. An extremely low dark current of <50 fA, limited by instrumentation, is achieved. This corresponds to a dark current density of <5.0 fA μm^{-2}, or 0.1 fA μm^{-2} found by fitting the IV curve, which to the best of our knowledge is the lowest for a nanowire or nanopillar based device. This low dark current is a testament of the excellent quality of the regrowth material, device design, and fabrication process. When illuminated by AM 1.5 G solar spectrum, the solar cell showed an open circuit voltage (V_{OC}) of 0.534 V, a short circuit current (I_{SC}) of 96.0 pA, and a fill factor of 48.2%. Normalizing I_{SC} to the projected exposed area yields a short circuit current density (J_{SC}) of 76.3 mA cm^{-2}. This is more than a factor of 2 higher than the J_{SC} of 32.2 mA cm^{-2} predicted by Shockley−Queisser limit for a planar solar cell. In principle, normalizing to the projected area could lead to a large error given that any tiny tilt to the device under test could result in a large variation in the projected area. However, we found a very weak angular dependence in the solar cell measurements that makes our efficiency calculation quite resilient to error. Even a 5° deviation of solar incident angle results in merely a 1.1% change in the I_{SC}; the angular insensitivity of the device makes the measurement tolerant to angular error. The more than twice higher J_{SC} is a result of the nanopillar antenna effect that makes the effective optical capture cross section larger than the physical cross section of the nanopillar. The power conversion efficiency of the single pillar device from the above figures of merit comes to 19.6%.

When the solar cell is cooled to a lower temperature, the V_{OC} increases monotonically and reaches 0.7 V at −100 °C (Figure 3c). The V_{OC} extrapolated to absolute zero following this trend is 0.94 V, which is a value substantially lower than the absorber band gap of 1.42 eV. Additionally, the p-doping level of the InP core was found to be rather low at 5×10^{15} cm^{-3} from a 4-point probe measurement (see Supporting Information, Section VII). Because of the low doping level, the core is expected to be depleted almost all the way to the root of the nanopillar. In that case, interfacial recombination at the type-II InP−silicon interface is a major nonradiative recombination pathway, which has a lower activation energy than the bandgap of the absorber.[35−37]This is consistent with the extrapolated V_{OC} being 0.94 eV instead of the absorber bandgap. Essentially, with a voltage penalty of 0.406 V from the extrapolated V_{OC} and a temperature coefficient for the V_{OC} of only 1.35 mV/K the device behaves as a good solar cell but with a lower bandgap. The effective bandgap corresponds to the type-II gap between silicon and InP at the interface, which acts as a heterostructure barrier.[36] Approaches to achieve a better device performance would require the elimination of interfacial recombination, potentially by increasing the doping near the nanopillar base so that the minority carriers are isolated from the interface. Solutions could involve switching to an n-core p-shell design or modifying the growth conditions for better in situ Zn incorporation. A higher doping in the core of the pillar would also prevent nonradiative recombination at the horizontally terminated defects near the base of the pillar, which were described in prior work.[18]

Figure 4a shows the external quantum efficiency (EQE) as a function of wavelength for the solar cell under direct, top-down illumination. Absorption enhancement effect can be clearly seen, as evidenced by the EQE value of 200−400% for the wavelength range of 400−800 nm. This suggests a dielectric antenna effect enhancing photon absorption over a broad wavelength range. The antenna enhancement effect allows efficient coupling of light into the resonator modes of the nanopillar,[28,29] allowing broadband, full solar spectrum absorption enhancement observed in the EQE data. The EQE data also shows insignificant absorption for wavelengths between 870 and 1100 nm, the band gap wavelengths of wurtzite phase InP and silicon, respectively, indicating that absorption in the silicon substrate does not contribute to the solar cell efficiency. The photocurrent map displayed in Figure 4b, generated by scanning a 2.4 μm wide 660 nm laser beam across the nanopillar solar cell, also reveals negligible photocurrent contribution from the silicon substrate. The spot size of 2.4 μm was measured separately using a knife-edge method.[30,31] As highlighted by the blue outline in Figure 4b, the resulting photocurrent spot has a full-width at half-maximum of ∼2.3 μm, which is simply the width of the excitation laser beam. This result proves that the photocurrent measured indeed comes solely from carriers generated within the InP nanopillar, as photocurrent was collected only when the laser spot was shone directly onto the nanopillar solar cell.

The dielectric antenna effect is evident in the I−V measurements of the solar cell at different illumination angles made onto the uncovered side of the nanopillar. As shown in Figure 5a,b, both measured V_{OC} and I_{SC} increase as the incidence angle increases (angle defined in the inset of Figure 5a). Although the increase in V_{OC} and I_{SC} are expected because the capture area of the solar cell increases with incidence angle, however, the amount of change is unexpectedly small. Instead of simply scaling proportionally to the capture area of the solar cell, the I_{SC} was found to increase by only a factor of 2.9 despite

DOI: 10.1021/acs.nanolett.5b00756
Nano Lett. 2015, 15, 4961−4967

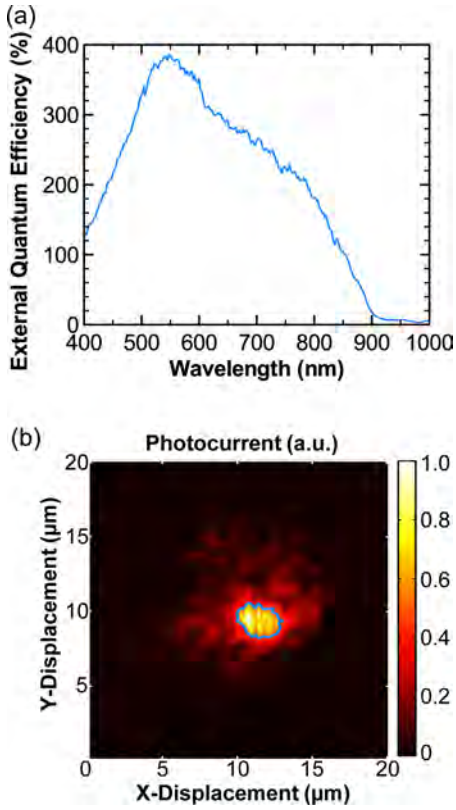

Figure 4. Single nanopillar solar cell external quantum efficiency and photocurrent map. (a) EQE of InP nanopillar solar cell with top-down illumination showing an enhanced EQE of 200−400% for most wavelengths. (b) A photocurrent spatial scan of the device was performed with a focused 660 nm laser to verify that the light absorption occurs at the III−V nanopillar and not the silicon substrate. The spatial full width half-maximum of both the photocurrent scan distribution (outlined in blue) and the focused laser spot (separately measured using a knife-edge method[30,31]) were found to be ∼2.4 um, confirming that the InP pillar is the light absorber. If the silicon were to absorb significantly, the photocurrent scan spot size would be substantially larger due to the diffusion of carriers from across the substrate to the device p−n junction.

a calculated 33 times increase in solar cell exposed capture area. This rather angle insensitive photovoltaic output is the result of the dielectric antenna effect enhancing optical absorption for near on-axis illumination,[29] which can be clearly seen in the J_{SC} plot in Figure 5c. The tapered sidewalls of the nanopillar also create a much stronger and tighter focusing effect for near on-axis illumination compared to nontapered nanopillars, allowing for much greater absorption enhancement for near on-axis illumination that would not have otherwise experienced with nontapered nanopillars.[32] Thus, the resulting much more pronounced enhancement effect for near on-axis illumination and the subsequent leveling off of this enhancement effect at higher incident angles compensate nicely for the change in the physical capture cross-section of the nanopillar solar cell, giving rise to its angle insensitive response. With further optimization on the taper angle and dimensions of the nanopillar, it is possible to create a nanopillar solar cell that is completely angle insensitive. Hence, it is clear that the antenna effect not only improves the solar cell performance but also enables illumination angle insensitive response. This allows solar cells made with tapered nanopillars to have reliable and steady power output without the need of expensive solar tracking system to adjust for sunlight angle of illumination changes during the day and throughout seasons.

Simulation of the solar cell structure with finite-difference time-domain modeling confirms our experimental results of enhancement due to dielectric antenna. Figure 6a shows the simulated I_{SC} as a function of incident angle, coplotted against the change in capture area. Again, the simulated I_{SC} changes much slowly and differently than the capture area of the solar cell. The simulated J_{SC} plot displayed in Figure 6b also confirms the antenna enhancement effect favoring near on-axis illumination as the source of the insensitive angular response. Although the enhancement effect for the micron-sized nanopillars is somewhat smaller compared to that of nanowires with deep subwavelength diameter,[5] the resulting lower surface-to-volume ratio reduces the impact of surface recombination, which is especially detrimental to the efficiency of III−V nanowire solar cells.[9,10] The antenna enhancement effect also makes the absorption cross-section appear bigger than the physical capture cross-section, allowing sparsely populated nanopillar array to absorb almost all of the incident sunlight. The simulation data plotted in Figure 6c clearly supports this claim with two InP nanopillar arrays absorbing 90% of the solar spectrum with merely 17% of the solar cell volume filled with nanopillars. And with the tapered sidewalls of the nanopillar creating more leaky resonator modes compared to nontapered

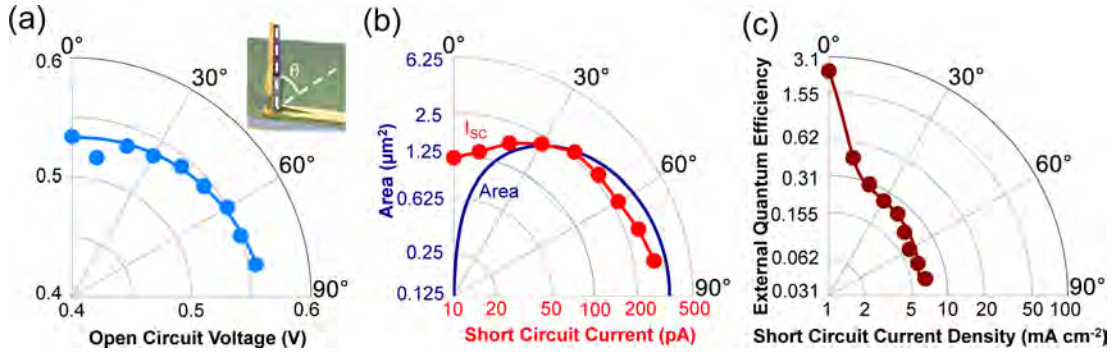

Figure 5. Measured angular response of a single nanopillar solar cell. (a) Device open circuit voltage V_{OC} as a function of illumination angle in polar coordinate. The inset shows how the illumination angle θ is defined with the respect to the nanopillar. (b) Experimentally measured short circuit current I_{SC} (red) shows angle insensitive response as it increased by a factor of 2.9 despite a 33-fold calculated increase in device capture area (blue) as the illumination angle was changed from 0° to 80°. (c) The short circuit current density J_{SC} reveals a tapered antenna enhancement effect that compensates for the change in capture cross-section as the angle of illumination is changed.

DOI: 10.1021/acs.nanolett.5b00756
Nano Lett. 2015, 15, 4961−4967

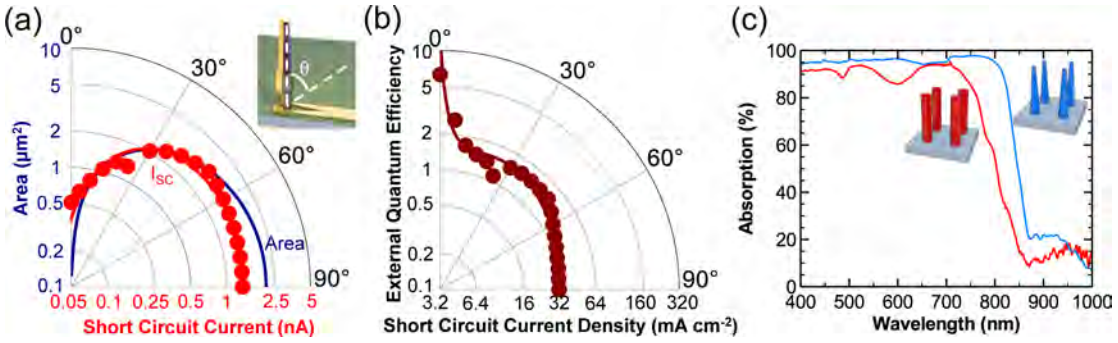

Figure 6. Simulated angular response of a single nanopillar solar cell and simulated absorption from a nanopillar array. (a) Simulated short circuit current I_{SC} (red) also shows angle insensitive response that scales very differently from the change in the capture area of the solar cell (blue). (b) Simulated short circuit current density J_{SC} confirms the directional antenna enhancement effect compensating for the change in capture cross-section as the illumination angle is changed. (c) Simulated absorption spectra of two nanopillar arrays showing greater than 90% absorption despite having only 17% volume fill ratio. The red curve shows the absorption spectrum of an array of 510 nm wide nontapered nanopillars that are spaced 1 μm apart. The blue curve shows the absorption spectrum of a nanopillar array with tapered sidewalls. The array with tapered nanopillars is able to absorb 95% of the light, compared to absorbing 90% of the light by the array of nontapered nanopillars. To keep the volume fill ratio the same at 17%, the tapered nanopillars have upper and lower diameters of 325 and 650 nm, respectively, and are 6 μm tall. Micro/nanopillars of this dimension can be easily achieved by scaling growth time. The tapered nanopillars in this array are also spaced 1 μm apart.

nanopillar,[33,34] light can be more readily coupled into the nanopillar body.[32] Thus, compared to nanopillar arrays with vertical sidewalls (red trace in Figure 6c), tapered nanopillar arrays (blue trace in Figure 6c) display higher light absorption at 95% (versus 90% by the nontapered nanopillar arrays), even when both arrays have the same 17% volume fill ratio. Therefore, solar cell efficiency can be further improved with tapered nanopillars.

Conclusion. In conclusion, we have demonstrated a single InP nanopillar solar cell grown on a silicon substrate with a high 0.534 V V_{OC}. The solar cell displays absorption enhancement at a factor of 200−400%, as observed from the external quantum efficiency, when illuminated top-down due to a novel tapered antenna effect. As a result of the enhancement and antenna effect, the solar cell output exhibits an interesting angle insensitive to photovoltaic characteristics, making it well-suited for low cost or no tracking system to adjust for sun ray directionality during the day and seasonal shifts. The tapered sidewalls and enhancement effect also allow sparsely packed nanopillar array to absorb almost all the sunlight, further reducing material cost of the solar cell. As a potentially highly efficient, incident angle insensitive solar cell grown on low cost silicon substrate, InP nanopillar solar cell can potentially be a game changer in making solar energy more affordable and widely deployed.

■ ASSOCIATED CONTENT

Supporting Information

More information on the nanopillar growth, device fabrication, photovoltaic characterization, exposed area calculation, and simulation and device performance improvement from re-growth. The Supporting Information is available free of charge on the ACS Publications website at DOI: 10.1021/acs.nanolett.5b00756.

■ AUTHOR INFORMATION

Corresponding Author

*E-mail: cch@berkeley.edu.

Author Contributions

All authors contributed significantly to this work, and the manuscript was composed with inputs from all authors.

W.S.K. and T.-T.D.T. contributed equally to this work.

Notes

The authors declare no competing financial interest.

■ ACKNOWLEDGMENTS

This work was supported by U.S. DOE SunShot DE-EE0005316, U.S. DOE Bay Area Photovoltaics Consortium DE-EE0004946, DoD NSSEFF Fellowship N00244-09-1-0013 and N00244-09-1-0080, NSF Award 0939514, and California Advanced Solar Technologies Institute, UC Multicampus Research Program and Initiatives (MRPI). The authors acknowledge the support of the National Center for Electron Microscopy, Lawrence Berkeley Laboratory for the use of their facilities.

■ REFERENCES

(1) LaPierre, R. R.; Chia, A. C. E.; Gibson, S. J.; Haapamaki, C. M.; Boulanger, J.; Yee, R.; Kuyanov, P.; Zhang, J.; Tajik, N.; Jewell, N.; Rahman, K. M. A. *Phys. Status Solidi RRL* **2013**, *7*, 815−830.
(2) Mårtensson, T.; Svensson, C. P. T.; Wacaser, B. A.; Larsson, M. W.; Seifert, W.; Deppert, K.; Gustafsson, A.; Wallenberg, L. R.; Samuelson, L. *Nano Lett.* **2004**, *4*, 1987−1990.
(3) Heurlin, M.; Wickert, P.; Fält, S.; Borgström, M. T.; Deppert, K.; Samuelson, L.; Magnusson, M. H. *Nano Lett.* **2011**, *11*, 2028−2031.
(4) Holm, J. V.; Jørgensen, H. I.; Krogstrup, P.; Nygård, J.; Liu, H.; Aagesen, M. *Nat. Commun.* **2013**, *4*, 1498.
(5) Krogstrup, P.; Jørgensen, H. I.; Heiss, M.; Demichel, O.; Holm, J. V.; Aagesen, M.; Nygard, J.; Fontcuberta i Morral, A. *Nat. Photonics* **2013**, *7*, 306−310.
(6) Glas, F. *Phys. Rev. B* **2006**, *74*, 121302.
(7) Wallentin, J.; Anttu, N.; Asoli, D.; Huffman, M.; Aberg, I.; Magnusson, M. H.; Siefer, G.; Fuss-Kailuweit, P.; Dimroth, F.; Witzigmann, B.; Xu, H. Q.; Samuelson, L.; Deppert, K.; Borgström, M. T. *Science* **2013**, *339*, 1057−1060.
(8) Yoshimura, M.; Nakai, E.; Tomioka, K.; Fukui, T. *Appl. Phys. Express* **2013**, *6*, 052301.
(9) Cui, Y.; Wang, J.; Plissard, S. R.; Cavalli, A.; Vu, T. T. T.; van Veldhoven, R. P. J.; Gao, L.; Trainor, M.; Verheijen, M. A.; Haverkort, J. E. M.; Bakkers, E. P. A. M. *Nano Lett.* **2013**, *13*, 4113−4117.
(10) Mariani, G.; Scofield, A. C.; Hung, C.-H.; Huffaker, D. L. *Nat. Commun.* **2013**, *4*, 1497.
(11) Shin, J. C.; Kim, K. H.; Yu, K. J.; Hu, H.; Yin, L.; Ning, C. Z.; Rogers, J. a; Zuo, J. M.; Li, X. *Nano Lett.* **2011**, *11*, 4831−4838.

DOI: 10.1021/acs.nanolett.5b00756
Nano Lett. 2015, 15, 4961−4967

(12) Heigoldt, M.; Arbiol, J.; Spirkoska, D.; Rebled, J. M.; Conesa-Boj, S.; Abstreiter, G.; Peiró, F.; Morante, J. R.; Fontcuberta i Morral, A. *J. Mater. Chem.* **2009**, *19*, 840−848.
(13) Gorji Ghalamestani, S.; Heurlin, M.; Wernersson, L.-E.; Lehmann, S.; Dick, K. a. *Nanotechnology* **2012**, *23*, 285601.
(14) Chuang, L. C.; Moewe, M.; Ng, K. W.; Tran, T.-T. D.; Crankshaw, S.; Chen, R.; Ko, W. S.; Chang-Hasnain, C. *Appl. Phys. Lett.* **2011**, *98*, 123101.
(15) Chuang, L. C.; Moewe, M.; Chase, C.; Kobayashi, N. P.; Chang-Hasnain, C.; Crankshaw, S. *Appl. Phys. Lett.* **2007**, *90*, 043115.
(16) Ng, K. W.; Tran, T.-T. D.; Ko, W. S.; Chen, R.; Lu, F.; Chang-Hasnain, C. J. *Nano Lett.* **2013**, *13*, 5931−5937.
(17) Ren, F.; Wei, N. K.; Li, K.; Sun, H.; Chang-Hasnain, C. J. *Appl. Phys. Lett.* **2013**, *102*, 012115.
(18) Ng, K. W.; Ko, W. S.; Tran, T.-T. D.; Chen, R.; Nazarenko, M. V.; Lu, F.; Dubrovskii, V. G.; Kamp, M.; Forchel, A.; Chang-Hasnain, C. J. *ACS Nano* **2013**, *7*, 100−107.
(19) Li, X.; Zhan, Y. *Appl. Phys. Lett.* **2013**, *102*, 021101.
(20) Kupec, J.; Witzigmann, B. *Opt. Express* **2009**, *17*, 10399−10410.
(21) Wang, X.; Kurdgelashvili, L.; Byrne, J.; Barnett, A. *Renewable Sustainable Energy Rev.* **2011**, *15*, 4248−4254.
(22) Mathieson, K.; Loudin, J.; Goetz, G.; Huie, P.; Wang, L.; Kamins, T. I.; Galambos, L.; Smith, R.; Harris, J. S.; Sher, A.; Palanker, D. *Nat. Photonics* **2012**, *6*, 391−397.
(23) Röger, M.; Böttger, G.; Dreschmann, M.; Klamouris, C.; Huebner, M.; Bett, a W.; Becker, J.; Freude, W.; Leuthold, J. *Opt. Express* **2008**, *16*, 21821−21834.
(24) Kayes, B. M.; Atwater, H. A.; Lewis, N. S. *J. Appl. Phys.* **2005**, *97*, 114302.
(25) Tran, T.-T. D.; Sun, H.; Ng, K. W.; Ren, F.; Li, K.; Lu, F.; Yablonovitch, E.; Chang-Hasnain, C. J. *Nano Lett.* **2014**, *14*, 3235−3240.
(26) Stellwag, T. B.; Dodd, P. E.; Carpenter, M. S.; Lundstrom, M.; Pierret, R. F.; Melloch, M. R.; Yablonovitch, E.; Gmitter, T. In *Effects of Perimeter Recombination on GaAs-Based Solar Cells*, Photovoltaics Specialist Conference, Kissimmee, FL, May, 21−25, 1990.
(27) Li, K.; Sun, H.; Ren, F.; Ng, K. W.; Tran, T.-T. D.; Chen, R.; Chang-Hasnain, C. J. *Nano Lett.* **2014**, *14*, 183−190.
(28) Grzela, G.; Paniagua-Domínguez, R.; Barten, T.; Fontana, Y.; Sánchez-Gil, J. a; Gómez Rivas, J. *Nano Lett.* **2012**, *12*, 5481−5486.
(29) Grzela, G.; Paniagua-Domínguez, R.; Barten, T.; van Dam, D.; Sánchez-Gil, J. a; Rivas, J. G. *Nano Lett.* **2014**, *14*, 3227−3234.
(30) Suzaki, Y.; Tachibana, A. *Appl. Opt.* **1975**, *14*, 2809−2810.
(31) Kimura, S.; Munakata, C. *Opt. Lett.* **1987**, *12*, 552−554.
(32) Gregersen, N.; Nielsen, T. R.; Claudon, J.; Gérard, J.-M.; Mørk, J. *Opt. Lett.* **2008**, *33*, 1693−1695.
(33) Chen, R.; Tran, T.-T. D.; Ng, K. W.; Ko, W. S.; Chuang, L. C.; Sedgwick, F. G.; Chang-Hasnain, C. *Nat. Photonics* **2011**, *5*, 170−175.
(34) Tran, T.-T. D.; Chen, R.; Ng, K. W.; Ko, W. S.; Lu, F.; Chang-hasnain, C. J. *Appl. Phys. Lett.* **2014**, *105*, 111105.
(35) While the manuscript was under review, an independent study on a similar subject was published: Nowzari, A.; Heurlin, M.; Jain, V.; Storm, K.; Hosseinnia, A.; Anttu, N.; Borgstrom, M. T.; Pettersson, H.; Samuelson, L. *Nano Lett.* **2015**, *15*, 1809−1814.
(36) Rau, U.; Schock, H. W. *Appl. Phys. A: Mater. Sci. Process.* **1999**, *69*, 131−147.
(37) Thompson, C. P.; Hegedus, S.; Shafarman, W.; Desai, D. In *Temperature Dependence of V_{OC} in CdTe and Cu(InGa)SeS_2-based Solar Cells*, Photovoltaics Specialist Conference, San Diego, CA, May, 11−16, 2008.
(38) Green, M. A. *Prog. Photovoltaics Res. Appl.* **2003**, *11*, 333−340.

DOI: 10.1021/acs.nanolett.5b00756
Nano Lett. 2015, 15, 4961−4967